27th EPS Conference on Contr. Fusion and Plasma Phys. Budapest, 12-16 June 2000 ECA Vol. **24B** (2000) 976 -979

Type-II ELMs and density peaking during high density H-modes on ASDEX Upgrade

J. Stober, O. Gruber, A. Herrmann, A. Kallenbach, M. Kaufmann, M. Maraschek, J. Neuhauser, F. Ryter, G. Sips, W. Treutterer, H. Zohm and the ASDEX Upgrade Team

Max-Planck-Institut für Plasmaphysik, EURATOM-Association, D-85748 Garching, Germany

Introduction

H-mode confinement according to ITERH-98(y) [1] is necessary for a next step device to reach its goals. Recently we have shown in ASDEX Upgrade, that this is possible also close to the Greenwald density if the triangularity δ is raised [2]. The main remaining problem with the H-mode is the pulsed power exhaust due to type-I ELMs, which leads to a too strong erosion of the divertor strike-point regions. As a solution, operation in the type-II ELM regime has been proposed, where the energy per ELM is significantly reduced [3,4,5]. Here we report studies on this favorable regime for the first time close to the Greenwald density.

A second topic of our high density H-mode studies is the increase of energy confinement with time in discharges with constant strong gas puffing, due to an increasingly peaking density profile with low Z_{eff}. These discharges which were run to study the scatter of confinement data obtained with density feedback control[2], contrast the generally observed trend of confinement degradation with density. To separate between central fueling and inward pinch as well as to check the compatibility with reactor relevant scenarios, heating power and heating methods have been varied.

Type-II ELMs

Fig. 1 shows, that small high-frequent ELMs have been observed on ASDEX Upgrade which show many features of type-II or grassy ELMs described for DIII-D [3], JT-60U [4] or during

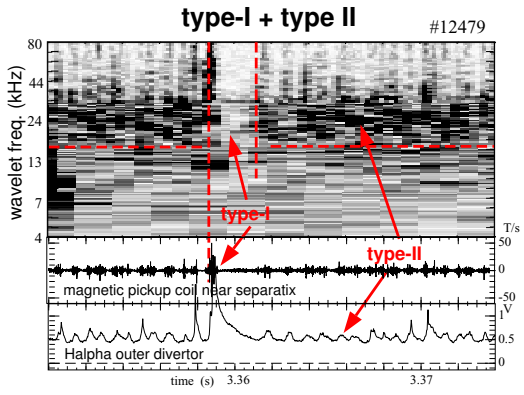

Figure 1: Mixed phase with type-I and type-II ELMs. The upper part shows the wavelet analysis of the magnetic signal shown in the middle. (I_p=1MA, q_{95}=4.0,, δ=0.36).

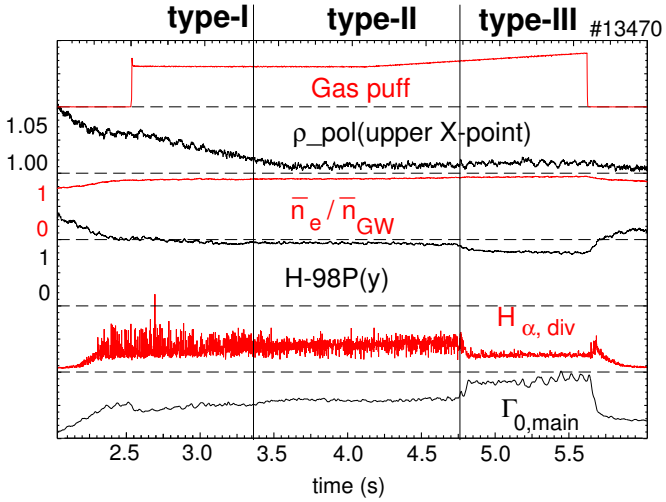

Figure 2: Three types of ELMs in one shot. The parameters used to change the type were the closeness to double null and the gas puff. (I_p=0.8MA, q_{95}=4.5, δ=0.40)

"Enhanced D_α" (EDA) [5] phases in Alcator C-Mod: The ELM amplitude of the H_α signal decreases, and frequencies between 0.5 kHz and 1 kHz are observed. The wavelet analysis of magnetic signals from probes close to separatrix shows ELM precursors in the frequency band between 15 kHz and 30 kHz as seen for ELMs during EDA phases. A threshold exists with respect to q_{95} (fig. 3B,C) and δ, i.e. we observe pure type-II phases only for $q_{95} \geq 4.5$ and $\delta \geq 0.4$ in accordance with [3,5] but ≈30 % lower than the values in JT-60U [4]. This might be connected with the observation that we get the type-II ELMs only at densities above $0.8 \times \bar{n}_{GW}$ and very close to a double null configuration as shown in fig. 2. Here the minimal difference between the flux surfaces through the x-points is ≈4 mm at the outer midplane. Fig. 2 also shows, that the upper density limit of this regime is given by a transition to type-III ELMs with a significant loss of stored energy. The type-II phase shows almost the same confinement as the type-I phase, an H-factor of 0.95 (ITERH-98(y)) at $0.95 \times \bar{n}_{GW}$. The thermography data of fig. 3 demonstrate clearly the advantage of the type-II regime which lies in a quasi-steady heat flux to the target plates. It is very convenient, that the density range one aims at for a next step device coincides with the easiest access to a type-II ELM regime. Fig. 3 demonstrates as well, that the H_α time trace is not always as conclusive as in fig. 1, but magnetic precursors (especially the wavelet analysis as shown in fig. 1) and target plate thermography allow a clear identification of a type-II phase. The transition from type-I ELM phases to type-II ELMs is not abrupt: Even at $\delta = 0.30$, not close to double null, several type-II ELMs can be found in between type-I ELMs, clearly identified by their magnetic precursor. If type-II ELMs appear, the time in between the type-I ELMs is increased (as compared to intervals without type-II). Comparing core and edge profiles for the time slices 2.7s (type-I) and 4.0s (type-II) in shots similar to fig. 2, no significant difference could be found ($\leq$ 5%) by edge thomson scattering and Lithium beam. A stability analysis of the edge is planned.

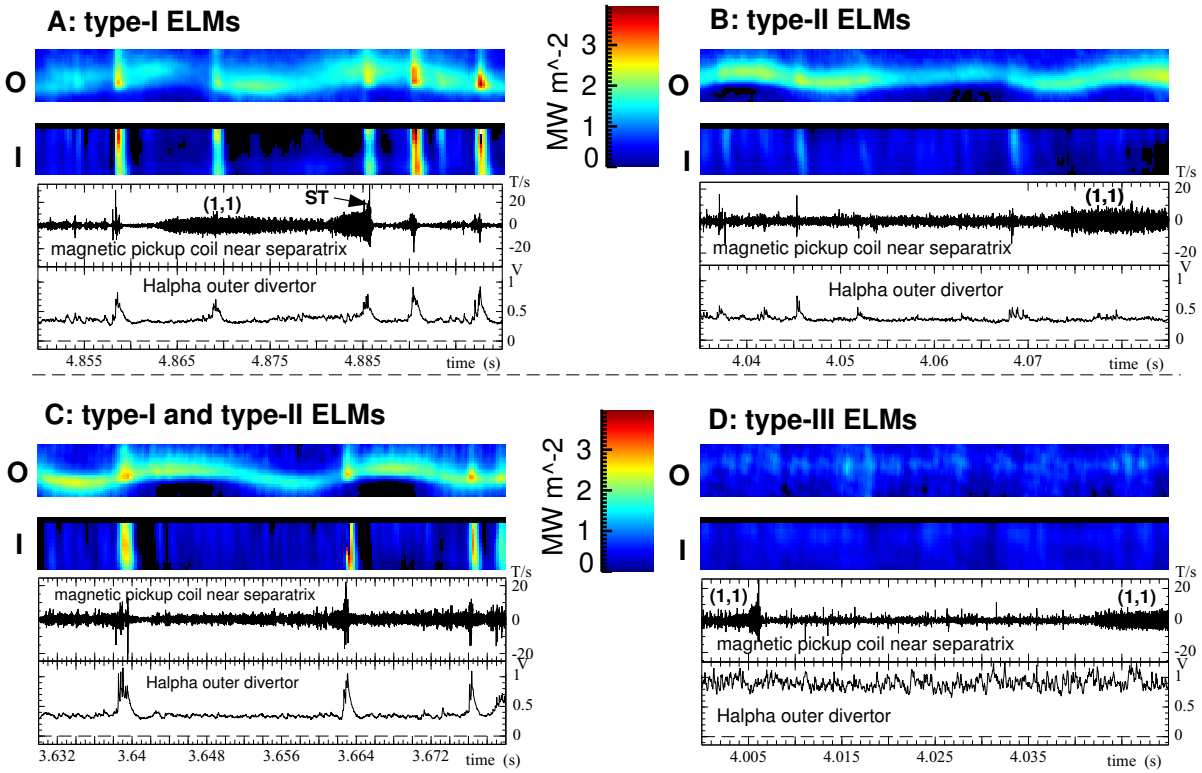

Figure 3: ELM types at I_p=0.8MA, δ=0.40. The magnetic and H_α signals as in fig. 1 are shown with the power flux close to the outer (O) and inner (I) strike points as measured by thermography [6]. Both areas shown are 7 cm wide. $\bar{n}_e \approx 0.9 \times \bar{n}_{GW}$. **A, B, D:** $q_{95} = 4.5$, **C:** $q_{95} = 3.9$.

Density Peaking

Fig. 4A,B shows the effect of density peaking and increase of confinement on a long time scale (i.e. $>20\ \tau_E$) observed for high density discharges and 5 MW NBI heating which exceed the Greenwald density significantly. This corresponds to recent results from DIII-D [7], where phases with even stronger peaking are terminated by MHD events. The pedestal and SOL regions remain unchanged during the density peaking as well as the T_e,T_i profiles over the whole radius. This is in consistency with earlier results from ASDEX Upgrade [8] showing that T-profiles are self-similar from the top of the pedestal to the center. An effect also known as profile stiffness. This effect, together with a flattening of the density profiles and a reduction of the pedestal pressure is the reason for the commonly observed decrease of confinement with increasing density, in contrast to the new results reported here. In the case of fig. 5A, the plasma performance and finally the peaking are limited by the loss of the sawteeth followed by accumulation of heavy impurities in the center.Before this accumulation Z_{eff} is below 1.3. Stiff temperature profiles are consistent with transport models for which the pedestal values determine the whole profile if the heating is strong enough to reach the critical gradient length $T/\nabla T$ [9]. For such models the heat conductivity χ is a function of the heat flux which could be changed by varying power and power deposition profile using NBI (slightly hollow heating profile) and ICRH (central heating). Fig. 4C compares the best performing time slice of fig. 4A (4.6s) to other heating scenarios which resulted in steady state plasmas after a few 100 ms. The peaking is reduced, if the plasma

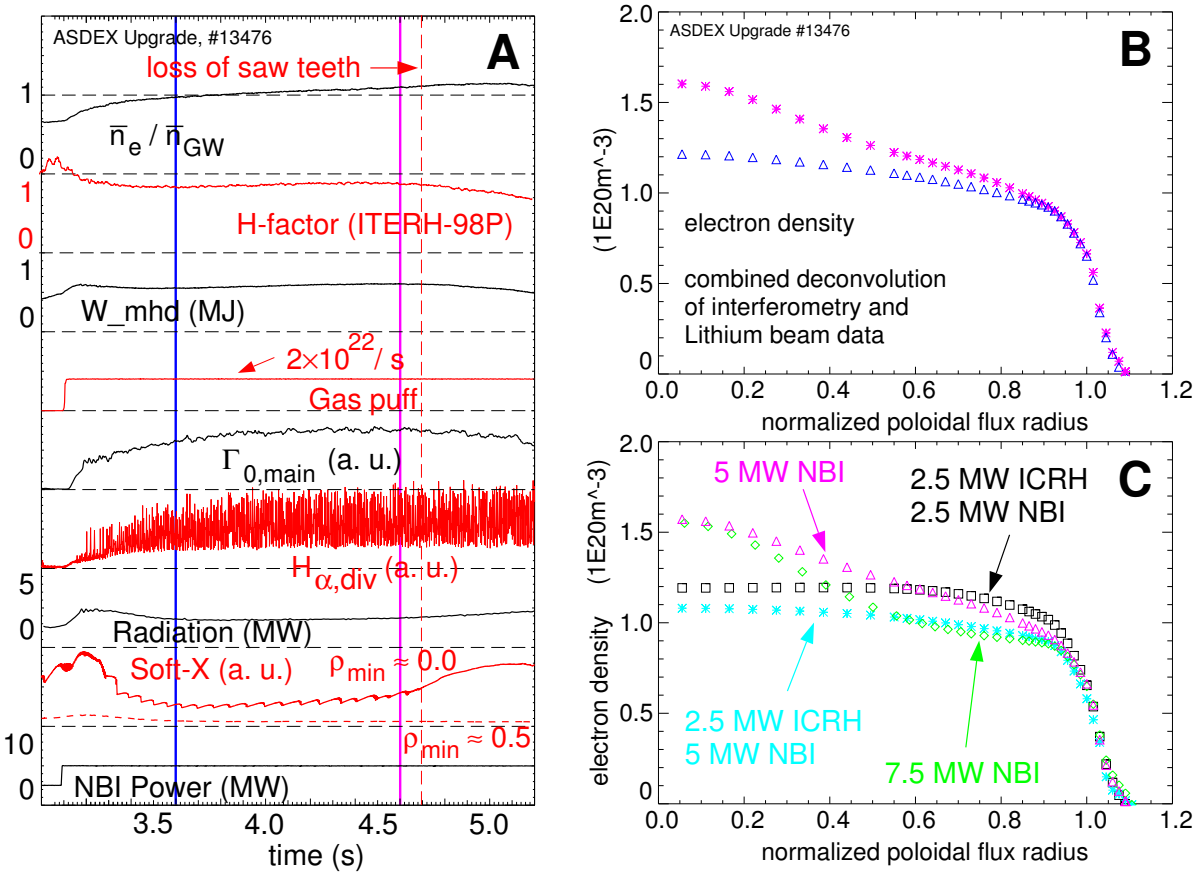

Figure 4: **A:** *time traces for a discharge with a strong constant gas puff (I_p=1MA, q_{95}=4.0, δ=0.30). The peaking of the density between 3.6s and 4.6s is shown in* **B**, *with corresponding colors.* **C** *compares the profile for 4.6s to those obtained with other heating scenarios. All others were steady state, i.e. without a uncontrollable peaking period of more than a second.*

is additionally heated with ICRH, i.e. 5 MW NBI and 2.5 MW ICRH. This implies that particle fueling of the NBI, which is unchanged, cannot be the only reason for the peaking. Therefore an inward particle pinch is involved. Increasing the heating by additional NBI power does not reduce the peaking but seems to shift it further inwards. Since the NBI heating-profile is expected to be slightly hollow the flattening seems to occur where the increase of the heat flux and also χ is strongest. The increase of χ is due to an effect known as power degradation in all scalings. The stored energy increases approximately as $\propto \sqrt{P}$. Indeed we measure the pedestal pressure to increases approximately this way and therefore χ increases also as $\propto \sqrt{P}$. The minimal peaking is observed if half of the NBI power is substituted by the ICRH, corresponding to much larger heat fluxes in the center. These four experiments together suggest a correlation between χ and the diffusion coefficient D in the sense that D is large where the heat flux and χ are large as already observed in [10]. If they are large enough the corresponding outward flux would cancel any inward pinch leading to flat profiles whenever the central heating is strong enough. A detailed transport analysis of our data is planed for the next months.

Conclusions

For the first time, the operation of a type-II ELMy H-mode close to the Greenwald density could be demonstrated. This offers a solution to main problems of a next step device: good confinement at high density and almost steady divertor load. It is achieved in a configuration with δ = 0.40 and depends critically on being close to a double null configuration. This indicates that the magnetic shear just inside the separatrix could be the relevant quantity for its occurrence. For the optimized configuration pure steady-state type-II H-modes without any type-I ELM were observed for values of q_{95} exceeding a threshold of $\approx$4.5.

Experiments with constant high gas puff revealed an increasing peaking of the density profile for more than 20 τ_E with constant pedestal and SOL profiles. Z_{eff} stays around 1.3 until the sawteeth disappear and heavy impurities accumulate and destroy this phase. T_i and T_e profiles do not change during the density peaking in accordance with their generally observed stiffness and the unchanged pedestal. Therefore the stored energy increases and H-factors above 1 are reached up to $1.1 \times n_{GW}$. The peaking is not only due to central fueling, so that an inward pinch of particles seems to exists. The deposition profile of the heating does change the peaking, in the sense that more central heating reduces the peaking. In terms of gradient length dominated transport the central χ increases if the heating is applied closer to the center. Our data suggest that this affects also the central D leading to a flattening of the profile. If this is true, the effect of density peaking is a challenge for any theory on particle transport but can not help to improve the confinement in a centrally heated fusion reactor.

References

[1] ITER Physics Basis, *Nucl. Fusion*, **39**, 2137, (1999)
[2] Stober, J. et al., *Plasma Phys. Control. Fusion*, **42**, A211, (2000)
[3] Ozeki, T. et al., *Nucl. Fusion*, **30**, 1425, (1990)
[4] Kamada, Y. et al., *Plasma Phys. Control. Fusion*, **42**, A247, (2000) and references therein
[5] Greenwald, M. et al., *Plasma Phys. Control. Fusion*, **42**, A263, (2000)
Greenwald, M. et al., *Physics of Plasmas*, **6**, 1943, (1999) and references therein
[6] Herrmann, A. et al., *Plasma Phys. Control. Fusion*, **37**, 17, (1995)
[7] Osborne, T.H. et al., *Plasma Phys. Control. Fusion*, **42**, A175, (2000)
[8] Suttop, W. et al., *Plasma Phys. Control. Fusion*, **39**, 2051, (1997)
[9] Tardini, G. et al., this conference
[10] Gruber, O. et al., *Plasma Phys. Control. Fusion*, **30**, 1611, (1988)